

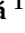



Article

Pneumatic Bellows Actuated Parallel Platform Control with Adjustable Stiffness Using a Hybrid Feed-Forward and Variable Gain Integral Controller

Martin Varga ¹, Ivan Virgala ^{1,*}, Michal Kelemen ¹, Ľubica Miková ¹, Zdenko Bobovský ², Peter Jan Sincak ¹ and Tomáš Merva ¹

¹ Faculty of Mechanical Engineering, Technical University of Košice, 040 01 Košice, Slovakia; martin.varga.2@tuke.sk (M.V.); peter.jan.sincak@tuke.sk (P.J.S.)

² Faculty of Mechanical Engineering, Technical University of Ostrava, 708 00 Ostrava, Czech Republic; zdenko.bobovsky@vsb.cz

* Correspondence: ivan.virgala@tuke.sk

Featured Application: The outcomes of this research can be implemented in the design of fast and easily tunable low-level controllers of redundant pneumatic parallel robots. This control algorithm allows for online stiffness changes of the robot, providing safe manipulation while maintaining the ability to use high amounts of force if needed.

Abstract: Redundant cascade manipulators actuated by pneumatic bellows actuators are passively compliant, rugged and dexterous, making them exceptionally well suited for application in agriculture. Unfortunately, the bellows are notoriously difficult to precisely position. This paper presents a novel control algorithm for the control of a parallel platform actuated by pneumatic bellows, which serves as a module of a cascade manipulator. The algorithm combines a feed-forward controller and a variable-gain I-controller. The mathematical model of the module, which serves as the feed-forward controller, was created by applying two simple regression steps on experimentally acquired data. The gain of the I-controller is linearly dependent on the total reference error, thereby addressing the prevalent problem of “a slow response or excessive overshoot”, which, in the described case, the simple combination of a feed-forward and constant-gain I-controller tends to suffer from. The proposed algorithm was experimentally verified and its performance was compared with two controllers: an ANFIS controller and a constant gain PID controller. The proposed controller has outperformed the PID controller in the three calculated criteria: IAE, ISE and ITAE by more than 40%. The controller was also tested under dynamic loading conditions, showing promising results.

Keywords: pneumatic bellows; parallel platform; feed-forward controller; variable-gain integral



Citation: Varga, M.; Virgala, I.; Kelemen, M.; Miková, Ľ.; Bobovský, Z.; Sincak, P.J.; Merva, T. Pneumatic Bellows Actuated Parallel Platform Control with Adjustable Stiffness Using a Hybrid Feed-Forward and Variable Gain I-Controller. *Appl. Sci.* **2023**, *13*, 13261. <https://doi.org/10.3390/app132413261>

Academic Editor: Luigi Fortuna

Received: 6 October 2023

Revised: 28 November 2023

Accepted: 29 November 2023

Published: 14 December 2023



Copyright: © 2023 by the authors. Licensee MDPI, Basel, Switzerland. This article is an open access article distributed under the terms and conditions of the Creative Commons Attribution (CC BY) license (<https://creativecommons.org/licenses/by/4.0/>).

1. Introduction

Industrial robots are an indispensable part of the manufacturing process in many industries, where their traits, i.e., precision, speed, and the ability to work basically nonstop, help increase productivity and decrease cost. It is therefore understandable, that there is a strong incentive to use industrial robots in other fields, like for example agriculture and medicine. The most common industrial robots are serial link 6R robots, 2R1T SCARA robots or parallel Delta robots driven by, most commonly, electric actuators, or in some cases hydraulic actuators [1]. These industrial robots were developed for many decades, their design is standardized, and their mathematical description and control design is fairly well researched. Unfortunately, these robots lack some key features needed in the aforementioned new fields of application. For example compliance, agility and complex modes of motion [2]. These requirements fulfil new emerging classes of robots i.e., redundant cascade and continuum robots [3]. Redundant robots are all those that have more degrees

of freedom than is necessary to perform a certain task [4]. Development of these robots accelerated after the year 2000. Redundant robots in general, but especially cascade and continuum robots, have unique characteristics. For example, according to [5,6], compliance, a good reach to weight ratio, modularity and other. These characteristics arise from their specific design.

In general, continuum and cascade robots consist of several in-series-connected parallel modules which, if underactuated, form a continuum robot and if fully actuated form a cascade robot. To describe the motion of a redundant robot and design a control algorithm for it, it is first necessary to focus on its individual modules and their properties. The chosen actuator type influences the achievable properties of a module. Electrical linear servo motors as used by [7] within the structure of a module or outside it, as by [8], provide high amounts of force and stiffness. Moreover, they are usually equipped with position sensors that simplify control. Hydraulic actuators, as seen in [9], provide high forces and can be precisely positioned, but are slow. Nonstandard actuators such as SMA springs, as seen in the work of [10], or dielectric materials, as described in [11], can also be used in this application. Pneumatic actuators are a popular class of actuators in cascade robot design. They provide high power density, have relatively low weight, and can be easily manufactured to custom specifications, as described in [1,12], or bought off the shelf in a variety of types and sizes [13–15]. In addition, the compressibility of air gives them a natural level of compliance. This property makes them the actuator of choice for medical applications, like for example in rehabilitation equipment [16] and flexible endoscopes [17,18], in agriculture [19], as parts in mobile robots [20,21], as the actuator for high-precision positioning systems [22] or as the stiffness regulating element in hybrid actuation schemes for continuum tendon driven robots as presented by [23].

There exist many well-known techniques that can be used to obtain robust controllers for complex systems, as described in [24]. Nevertheless, the control of a parallel platform module actuated by three or four pneumatic actuators remains a challenging task. One approach to controlling of these modules is to use a feed-forward controller alone or in combination with other types of controllers. The authors of [25] presented a modelling framework to design a model from which a feed-forward controller with satisfactory performance was developed. Ref. [26] developed a custom bellows-type actuator and applied it in a parallel platform with three degrees of freedom. Their control algorithm was a feed-forward controller based on an experimental mapping between pose, external forces and input pressure. In [27], the authors used a feed-forward controller based on a mathematical model in combination with a variable P-gain PI controller to combat the effect of hysteresis in the system. Ref. [28] uses a model-based controller with both feed-forward and feedback components with a structure similar to a PD controller to position a soft robot. Similarly ref. [29] used feedback linearisation to decouple the actuators of a soft pneumatic robot manipulator to achieve very precise and dynamic movements. The controller for this application was a model-based, feed-forward controller combined with a low gain PD controller. In [30], a planar platform actuated by pneumatic muscles was controlled using three fuzzy controllers synchronized through an ANFIS (adaptive neuro-fuzzy inference system)-based controller. Ref. [15] applied a simple constant-gain PID controller for positioning of a parallel platform actuated by four pneumatic muscles. The authors of Ref. [31] have demonstrated a nonlinear SMC (sliding-mode controller) based on a PID-type sliding surface combined with a lumped element model-based controller to control a soft pneumatically actuated robot. In [32], the authors use a fourier series-based adaptive sliding-mode controller with H_∞ tracking performance to address the high non-linearity and time-varying problem in a parallel platform actuated by rod-less pneumatic cylinders. while dealing with a tendon-driven redundant manipulator, the authors of Ref. [33] proposes a population-based model-free control method that could be applied to pneumatically actuated manipulators.

Based on our previous work we have set out to develop the mechanical design and control system for a rugged redundant cascade manipulator driven by pneumatic bellows,

intended for both research and agricultural use. The most difficult part of the development was the controller design for each separate module, as noted in previously mentioned articles. This task is notoriously difficult due to the inherent nonlinear hysteresis behaviour of the chosen actuator type and MIMO system as a whole. In previous research, a similar approach to in pneumatic parallel platform module control was taken by relying on experimental data. This concept was expanded upon by applying two regression steps to the data to obtain a mathematical model of the module, which took the place of a feed-forward controller. This feed-forward controller was then supplemented by a variable gain I-controller that facilitates disturbance rejection. The gain of the I controller is time-varying, allowing for specific adaptation dependent on the control error. The advantages of the ability to dynamically change the gains of a PID controller have been demonstrated by many authors. For example [34] presents a sigmoid-based variable coefficient PID where a modified sigmoid function is used to limit the variability of the PID controller coefficients in a predefined range. Refs. [34,35] added a nonlinear sine cosine algorithm to tune the coefficients of the PID controller. Ref. [36] utilized reinforcement learning and gain scheduling to tune the coefficients of their PID controller.

Here, we present a hybrid controller design which, allows for a on demand change in stiffness of the system during operation and lends itself well to be a part of complete control system for the whole cascade manipulator.

Based on previous papers survey, the novelty of the paper can be defined as follows:

- Development of a novel hybrid FFvI controller (Feed-forward variable gain integral controller) with time-varying gain and experimentally derived model using two regression steps;
- Establishment of controller design methodology for cascade redundant robots;
- Experimental positioning analyses under dynamic disturbance effects.

This paper focuses on the development of a novel controller for a 2 DOF pneumatic parallel platform that represents one module of the pneumatic manipulator PneuTrunk (see Figure 1), developed by our ARM-Lab. The first part of the paper presents the design and kinematic model of one module of PneuTrunk. In the second part, a feed-forward controller based on an experimentally identified system with stiffness regulation capabilities combined with a error dependent variable gain I controller for disturbance rejection is presented. In the third part, the proposed controller is compared with a simple PID controller and ANFIS controller. The reason for adopting an experiment driven controller design for this application when very robust alternatives in the form of model based feed-forward controllers, see [29], already exist is that in some cases a mathematical model is difficult or impractical to obtain. As an example, soft robots with complex couplet internal structures can be named. For these cases, our approach will be valid. As another benefit, this controller has the potential for periodic self-tuning, based on real online data gathered during use.



Figure 1. CAD model of PneuTrunk.

2. Design of PneuTrunk Module

As can be seen in Figure 1, the redundant manipulator PneuTrunk is a cascade type manipulator constructed out of parallel platform modules ordered in series. The number of modules depends on the required degrees of freedom. One module, shown in Figure 2, consists of two duraluminium plates connected by an universal joint and three evenly spaced pneumatic bellows. The tilt angles between the top and the bottom plates are measured by two potentiometric rotation sensors, placed in such a way that the axis of the universal joint is colinear with both axes of the sensors and the y sensor axis is always

parallel to the bottom plate and the x sensor axis is always parallel to the top plate. The pneumatic actuators are off-the-shelf Dunlop 2 3/4 × 3 bellows. The pressure in the pneumatic bellows is controlled by three separate electro-pneumatic pressure controllers SMC ITV1050-31F20. In our experience, these controllers have little lag and no discernible overshoot. All tubing is of inner diameter of 6 mm to eliminate the effects of tubing diameter on the dynamic behavior of the bellows. The module is controlled by a B&R PLC type 4PPC70-0702-20B and was programmed using B&R Automation studio version 4.9.

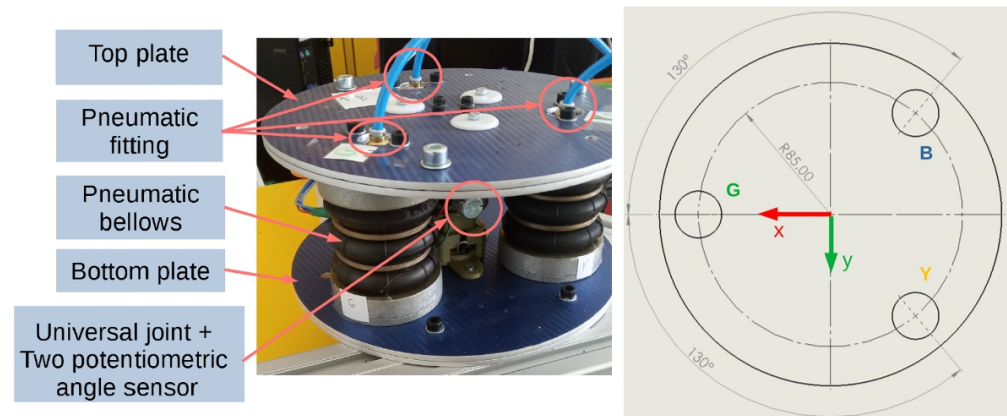


Figure 2. One module of the manipulator PneuTrunk and top sketch of the module. Letters G, B, Y denote the center-points of the bellows.

The maximum operating pressure for one bellows is 7 bar, but to prevent damage to the system and especially the universal joint, the allowable pressure range is set to 0–5 bar. The x -axis is oriented towards the center of one bellows. The asymmetric layout of the bellows with respect to the axes x and y in combination with the mechanical limits of the bellows themselves, causes the rotational extremes around both axis to be different, as can be seen in Table 1.

Table 1. Tilt extremes.

axis	Tilt [deg]	
	min	max
y	−24.4	16.6
x	−21.2	20

It is expected that the module will be driven only by positive pressure. This has important implications when designing the control algorithm for such a device. While the extension of one bellows is facilitated by simply supplying pressure, compression is achieved by applying external forces that predominantly originate from the extension of one or both remaining bellows. This fact is also the reason why the minimum number of pneumatic bellows is three. Coincidentally, because the module only has two degrees of freedom, this design is inherently overactuated. This causes one posture of the module to be reachable by an infinite number of bellows input pressure combinations and, in theory, giving the system the ability to change its stiffness without changing the posture. This was taken into account when designing the control algorithm for one module.

The flow of information and energy is visualized in Figure 3. The whole system is simple and contains only the necessary components. It could be argued that adding a center closed 2/2 valve between each bellows and its corresponding electropneumatic pressure controllers could give the system the ability to pneumatically lock the bellows extension, improving the systems positioning performance. Unfortunately, this would also complicate the system and its regulation, introducing other challenges and distracting from the aim of this paper.

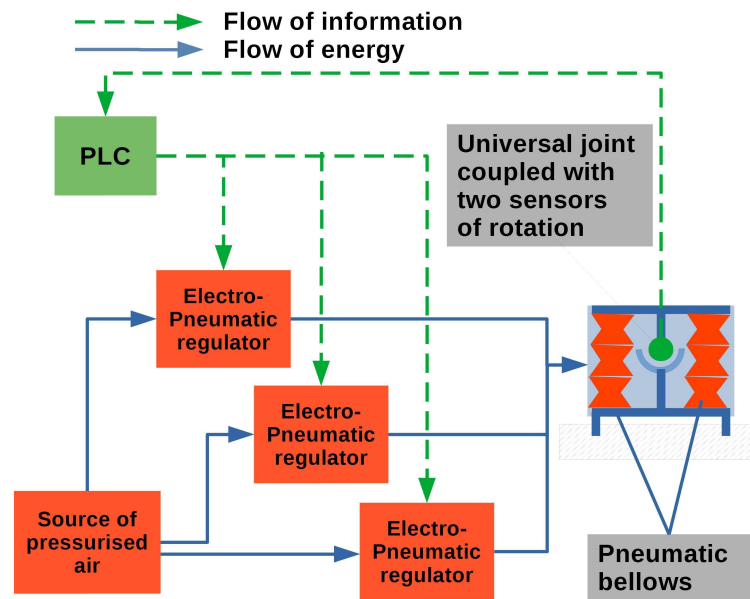


Figure 3. Flow of information and energy.

3. Mathematical Modeling

3.1. Mathematical Model of One Module

An important step before attempting to design a controller for a module is, to create an inverse kinematic model of the module first. In other words, to find a way to map the desired output parameters to the input parameters; in this case, the tilting angles to the extension/contraction of the bellows, see Figure 4. Inspiration is taken from the work of [37], where bellows-type actuators are represented by two elements connected by a translational joints and connected to the bottom and top plate by universal joints. This approach greatly simplifies kinematic modelling. For the purpose of modelling the dynamics of an actuator, the model needs to be augmented by adding torque on both universal joints that represent resistance to bending of the actuator.

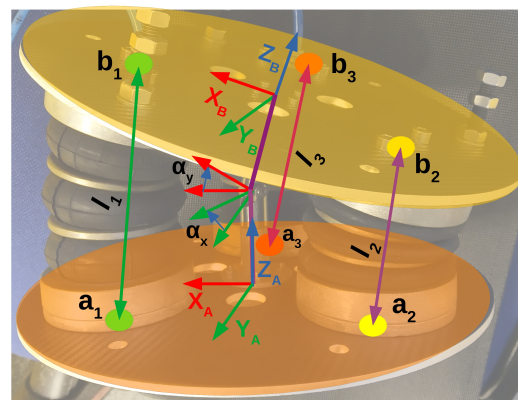


Figure 4. Schematic representation of the pneumatic module

For our design, there exists a closed form solution to inverse kinematics in the form of

$$l_i = | \mathbf{a}_i - \mathbf{H}_t \mathbf{b}_i(\alpha_x, \alpha_y) | \tag{1}$$

$$\mathbf{H}_t = \mathbf{T}_{z01} \mathbf{R}_{y12} \mathbf{R}_{x23} \mathbf{T}_{z34} \tag{2}$$

where $i \in \{1, 2, 3\}$ denotes the bellows, $\mathbf{a}_i \in \mathbb{R}^3$ are the coordinates of the center of the bellows on the bottom plate, $\mathbf{b}_i \in \mathbb{R}^3$ are the coordinates of the center of the bellows on the top plate, l_i is the distance between point \mathbf{a}_i and \mathbf{b}_i . Matrix $\mathbf{H}_t \in \mathbb{R}^{4 \times 4}$ represents

the transformation matrix between the fixed coordinate frame $x_a y_a z_a$ and the top plate coordinate frame $x_b y_b z_b$. $T_{z01}, T_{z34}, R_{x23}, R_{y12} \in \mathbb{R}^{4 \times 4}$ where T_{z01} is the translation matrix between the base frame and a parallel but offset frame $x' y' z'$, R_{y12} is the rotation matrix rotating frame $x' y' z'$ around its y axis by α_y into $x'' y'' z''$, R_{x23} is the rotation matrix rotating frame $x'' y'' z''$ around its x axis by α_x into $x''' y''' z'''$ and T_{z34} is the translation matrix between the frame $x''' y''' z'''$ and a parallel but offset top plate frame $x_b y_b z_b$, see Figure 5. Angle α_x is the tilt angle of the top plate around axis x and α_y is the tilt angle of the top plate around axis y .

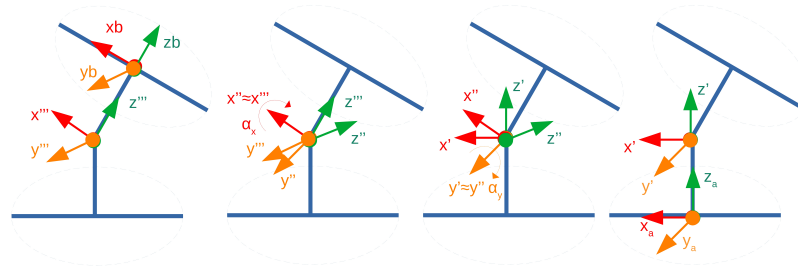


Figure 5. Transformation steps between frame $x_a y_a z_a$ and $x_b y_b z_b$

The role of the established kinematic model in relation to the posture control of the module described in later chapters is a central one. The goal of posture control of the platform is achieved indirectly by controlling the extension and total pressure in the respective bellows. The presented inverse kinematic model converts the reference tilt and actual tilt sensed by rotation sensors into the required extension/contraction and actual deformation of the bellows.

3.2. Model of Pneumatic Bellows

A pneumatic bellows is a linear pneumatic actuator consisting of a bellows type body and mounting flanges. The free length of the bellow is dependent on the difference between the ambient pressure and the pressure inside the bellows. From a physical point of view, the pneumatic bellows is a pneumatic spring with variable equilibrium length. The equilibrium length is dependent on the geometric and material properties of the bellows and the internal pressure within the bellows Figure 6.

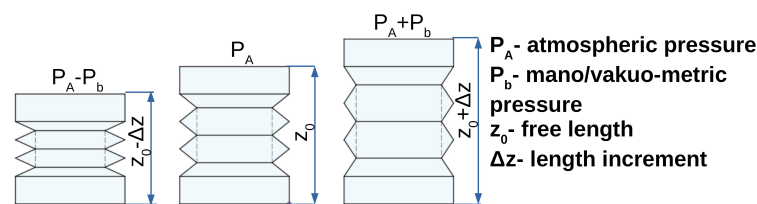


Figure 6. Bellow length in dependence on internal pressure.

The bellows can be modelled using the standard mass, spring, damper model represented by Equation (3), see Figure 7. The dominant force on the system is the spring force. The spring force is dependent on the pneumatic spring stiffness and the equilibrium height of the bellows at the current internal pressure. Equation (4) shows this relationship. Without being pressurized, the bellow behaves like a spring whose stiffness depends on the shape of the bellow. The current material properties that are also dependent on other factors like ambient temperature. Therefore, if the bellows are deformed, a spring force appears in the direction opposing the deformation. The equilibrium length is the length of the bellows at which the deformation force from the internal pressure is at equilibrium with the spring force. It can be seen that, the equilibrium height is a nonlinear parameter that depends on multiple other coupled parameters. Therefore, instead of a physical modelling approach, the model for the equilibrium height was derived from experimental data by

measuring the equilibrium height at different internal pressures; see Figure 8. The data was then approximated by a third-order polynomial function resulting in Equation (5).

$$F_M + F_b + F_k(k_p, P_b) + F_o = 0 \tag{3}$$

$$F_k = k_p(z_e(F_k, P_b) - z_r) \tag{4}$$

$$z_e = 0.45P_b^3 + 5.6P_b^2 + 23P_b + 1200 \tag{5}$$

where F_M is the inertial force, F_b the is damping force, F_k the is pneumatic spring force, F_o is outside the disturbance force, k_p is the pneumatic spring stiffness, P_b is internal the pressure, z_e is the equilibrium length, z_r is the actual length and F_m is the material spring force.

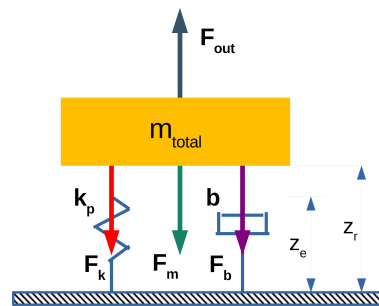


Figure 7. Mass-spring-damper model of pneumatic bellows.

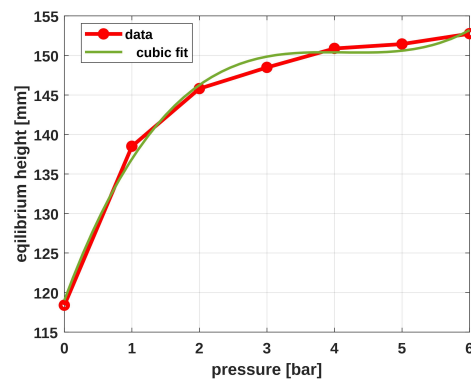


Figure 8. Relationship between internal pressure and Equilibrium height.

To create a simulation model of a pneumatic spring, it is necessary to determine the stiffness of the spring. This parameter can be derived from the Equations (6)–(8).

$$k_p = \frac{dF_k}{dz} \tag{6}$$

where

$$F_k = (P_0 - P_A)A \tag{7}$$

Assuming that the change in bellows internal volume is polytropic we get

$$P_0V^2 = constant \tag{8}$$

Combining the above equations

$$k_p = \frac{P_0 n A^2}{V} + P_B \frac{dA}{dz} \tag{9}$$

where V is total volume of air within the bellows and corresponding pneumatic tube, P_0 is the absolute pressure inside the bellows, A is an effective surface of the bellow, n is polytropic constant. The movement of the platform is expected to be slow, therefore we can approximate the process to be isothermal, hence $n = 1$. According to Equations (3)–(9) a simulation model in MATLAB version R2021b was developed.

The results of this model were compared with experimental data, where the bellow was pressurized to different pressures, a positive extension force was applied to the bellow and the total extension was measured. The results are in Figure 9.

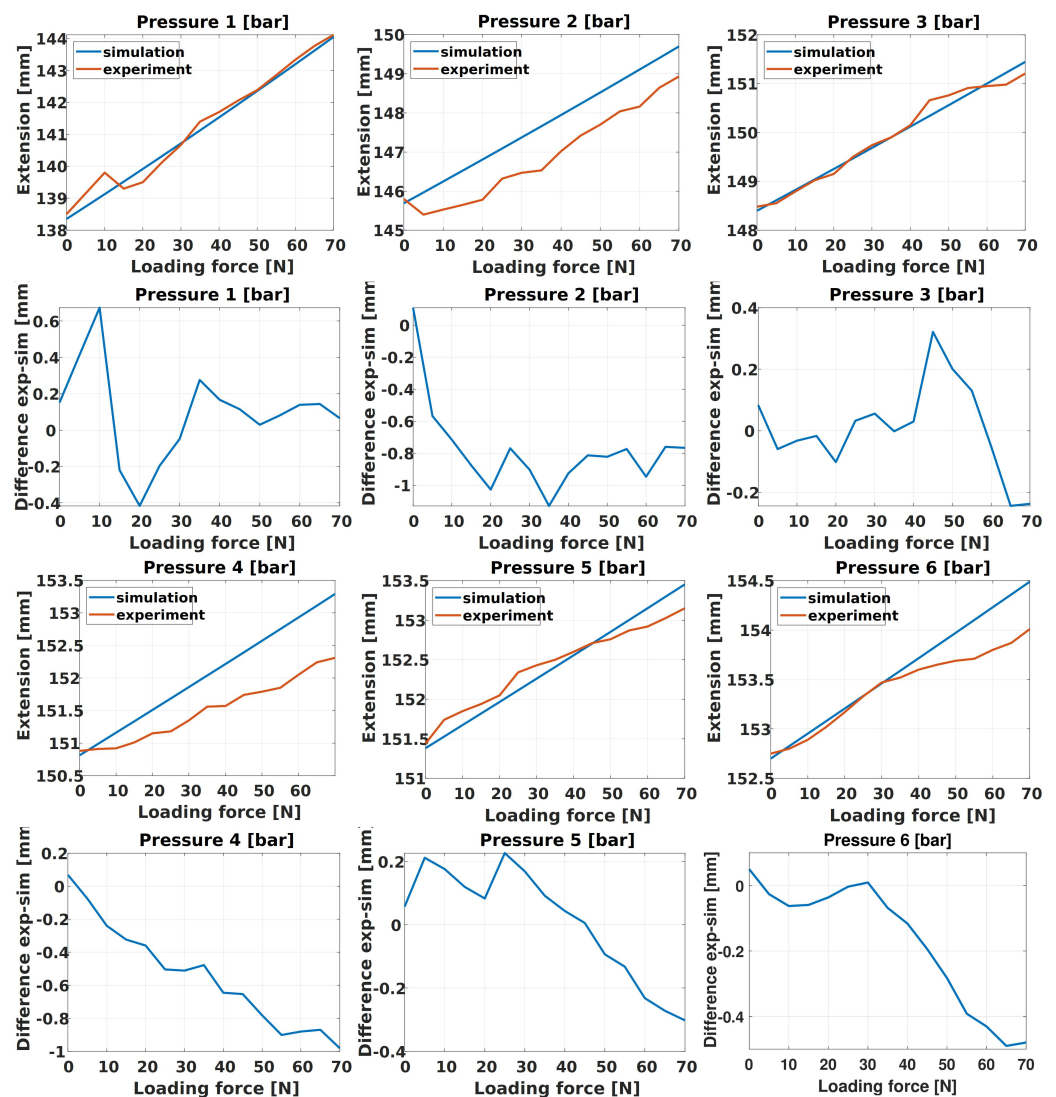


Figure 9. Experiment vs. simulation (1st and 3rd row) and the difference between simulation and experiment (2nd and 4th row).

The model of a pneumatic bellow gives satisfactory results. The maximum deviation for pressures between 1 bar and 6 bar does not exceed 1 mm, while for pressure 0 bar the deviation is nearly 4 mm, which points to either a measurement error or to some unknown effect that is much less pronounced in higher pressures.

This model represents the static behaviour of an air bellow performing linear deformation. It does not capture its bending behaviour or its dynamics. To be able to design a controller for one module of the manipulator PneuTrunk, it is necessary to also have a basic understanding of the dynamic behaviour of one bellow. This can be seen in the step response of one bellow to an input pressure step of 5 bar, shown in Figure 10.

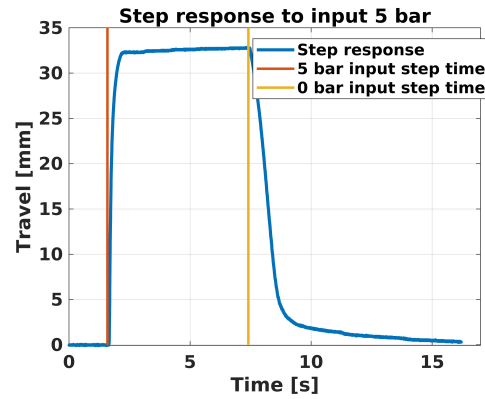


Figure 10. Step response of one bellows to step input 5 bar.

There is no discernible overshoot and the rise time from 0 s to maximum value is about 0.4 s. This means that the system is overdamped and 0.4 s represents the maximum possible regulation speed. It is also important to note the behaviour of the bellows when going back from 5 bar to 0 bar, where the actuator is passively returning to the original length. Here, not even after 8 s does the actuator reach the original length.

One important property of a pneumatic bellow, as noted by [38], is its hysteresis behaviour, where inflating and deflating a bellow results in a different free length at zero internal pressure. In our experiments, this behaviour resulted in a deviation of ± 2 mm. To combat this effect, the bellow was forced by an external stop to always be extended at zero internal pressure securing a stable free length. Creating a comprehensive bellow model falls outside the scope of this paper and will be a topic of further research. Nevertheless, it gives important insights into the behaviour of one bellow regarding controller development.

4. Controller Design

Controlling the posture of one module requires the combined effort of all three of its bellows actuators. The presented controller is designed to deal both with the non-linearity of the actuators and the over-actuation of the system. We define the controller consisting of two parts, a feed-forward controller and a variable gain I-controller (FFvI) see Figure 11.

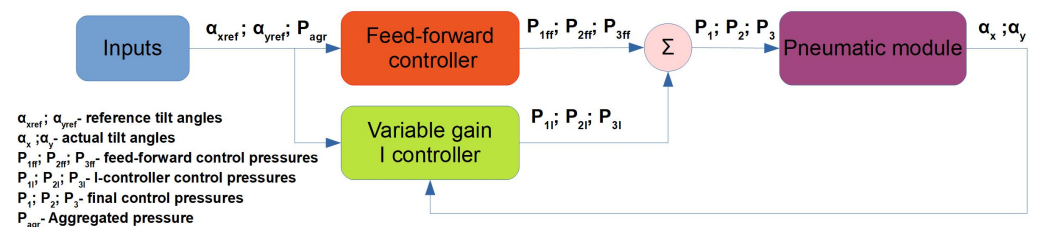


Figure 11. Block diagram of FFvI regulator.

The feed-forward control is widely used in research for these applications, for example, Refs. [25,26]. It uses an inverse model of a controlled system without a feedback loop. For this application, it will provide the rough estimate input. This leverages the lack of overshoot of the actuators even at large input pressure steps, as can be seen in Figure 10, it maximizes the controller speed, and it is generally easy to design and implement. As will be shown later, this system can also be driven by a pure constant gain PID controller, but a feed-forward controller is faster and has fewer errors. On the other hand, because

of its lack of a feedback loop, as seen in [25], it is unable to compensate for disturbance forces and system-model deviation. These are the reasons why the feed-forward controller is supplemented by a variable gain I-controller designed to complement the feed-forward controller and dynamically react to any differences between the reference values and actual values of the controlled variables.

4.1. Feed-Forward Controller Design

The feed-forward controller developed in this paper was designed using experimental data. Various pressure combinations were supplied to each bellows and the resulting posture was measured. The supplied pressures ranged from 0 bar to 5 bar with a 0.2 bar increment. This results in 18275 different pressure combinations and their corresponding tilt angles. The module workspace can be seen in Figure 12.

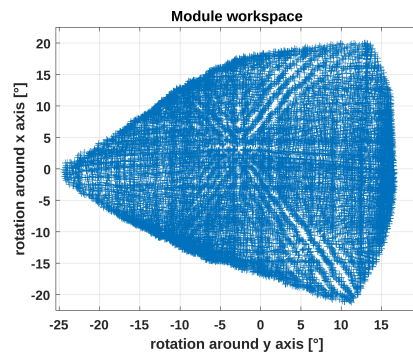


Figure 12. Module workspace.

The pointcloud matrix structure is organized as seen in Equation (10)

$$P_{PC} = [\alpha_x, \alpha_y, P_{1C}, P_{2C}, P_{3C}] \tag{10}$$

where α_x and α_y are the measured stable tilt angles which are the result of corresponding input pressures for the respective bellows P_{1C} , P_{2C} and P_{3C} .

Because of over-actuation and the parallel nature of the module design, one orientation of the module is achievable by an infinite combination of input pressures. This can be seen in Figure 13. Here the x -axis and y -axis are the tilt about the respective axis in degrees and the z -axis is the aggregate pressure, which is the sum of all bellows input pressures in bars. A higher aggregate pressure corresponds to a higher mechanical stiffness of the system. The control algorithm needs to take this into account.

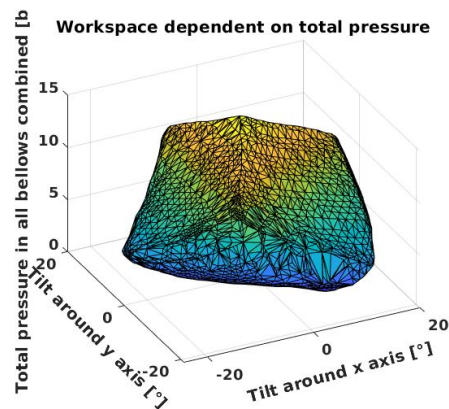


Figure 13. Aggregate pressure augmented workspace.

The experimentally measured data represents points in aggregate pressure-augmented workspace. To find the inlet pressures from the measured point-cloud, Algorithm 1 was applied.

Algorithm 1 Extract required bellows input pressures from point cloud

Input: Reference tilt angles α_{xref} , α_{yref} , required aggregate pressure level P_{agr} and $P_{PC} = [\alpha_x, \alpha_y, P_{1C}, P_{2C}, P_{3C}]$

Output: Required bellows input pressures P_1 , P_2 and P_3 to reach α_{xref} and α_{yref}

while isEmpty(Region) **do**

 Add all points to Region that pass the criterion:

$$\sqrt{(\alpha_{xcloud} - \alpha_{xref})^2} \leq anT \ \& \ |P_{1cloud} + P_{2cloud} + P_{3cloud} - P_{agr}| \leq aggrT$$

if isEmpty(Region) **then**

$anT = anT + incrementAngle$

$aggrT = aggrT + incrementPressure$

end if

end while

 Find point $Q \in Region$ with minimal expression

$$\sqrt{(\alpha_{xregion} - \alpha_{xref})^2 - (\alpha_{yregion} - \alpha_{yref})^2}$$

if $\sqrt{(\alpha_{xQ} - \alpha_{xref})^2 - (\alpha_{yQ} - \alpha_{yref})^2} \leq acceptableTol$ **then**

$$[P_1, P_2, P_3] = [P_{1Q}, P_{2Q}, P_{3Q}]$$

else

$$[P_1, P_2, P_3] = [mean(P_{1r}), mean(P_{2r}), mean(P_{3r})]$$

end if

Region-matrix of measured input pressures and corresponding posture that will be used to calculate the ended required input pressures to reach the desired posture; *anT*-maximum Euclidean distance of a measured point from the reference point in the augmented workspace in the $\alpha_x \alpha_y$ plane to be eligible for inclusion in *Region*; *aggrT*-maximum Euclidean distance of a measured point from the reference point in the augmented workspace along the aggregate pressure axis to be eligible for inclusion in *Region*; *incrementAngle*-increment to expand *anT* in case the previous search yielded empty *Region*; *incrementPressure*-increment to expand *aggrT* in case the previous search yielded empty *Region*.

Algorithm 1 will already supply a set of usable input pressures. Unfortunately, the results are influenced by the errors in measurement and effects of hysteresis. In a smooth trajectory tracking task, this can produce erratic, non-smooth input pressures. To solve these issues, the above Algorithm 1 was supplied with a set of reference angles ranging from -10° to 10° with an increment of 0.05° for both α_x and α_y and a constant aggregate pressure P_{agr} . The result is three 3D meshes representing the relationship between the reference angles and the three input pressures separately. These meshes were then separately approximated as a surface using a second order x and second order y surface plot. The result for input pressure 1 can be seen in Figure 14 and the equation describing this surface is Equation (11)

$$P_1 = 2.964 - 0.1113\alpha_x + 0.000344\alpha_y + 0.000726\alpha_x^2 + 0.00407\alpha_x\alpha_y - 0.00123\alpha_y^2 \quad (11)$$

This process was repeated for aggregate pressures between 3.6 bar and 15 bar with increments of 0.6 bar for all three bellows. The result is a set of smooth surfaces representing the complete augmented workspace, see Figure 15 for bellows 1.

The coefficients describing all the surfaces can be further interpolated to get six equations approximating the complete aggregate pressure augmented workspace. The coefficients were interpolated by a 7-th order polynomial. Figure 16 compares the output of Algorithm 1 and the interpolated feed-forward controller. The output of Algorithm 1 follows the smooth reference signal, but it shows non-smooth, erratic step behavior, while the output of the interpolated feed-forward controller is smooth.

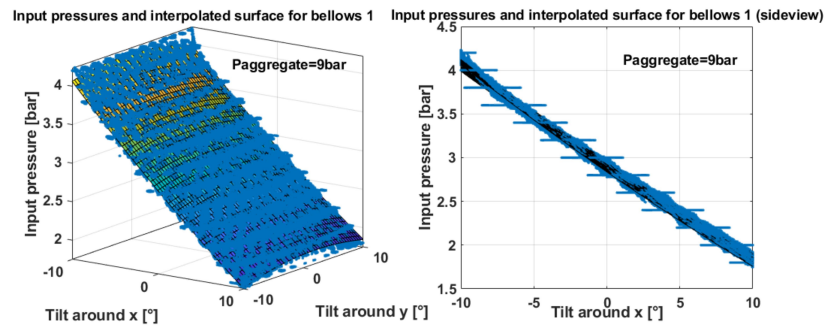


Figure 14. Calculated input pressures and approximated surface for bellow 1.

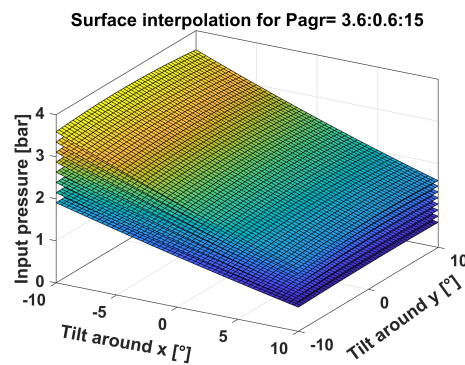


Figure 15. Surface approximation for $P_{agr} = 3.6:0.6:15$ [bar] for bellows 1.

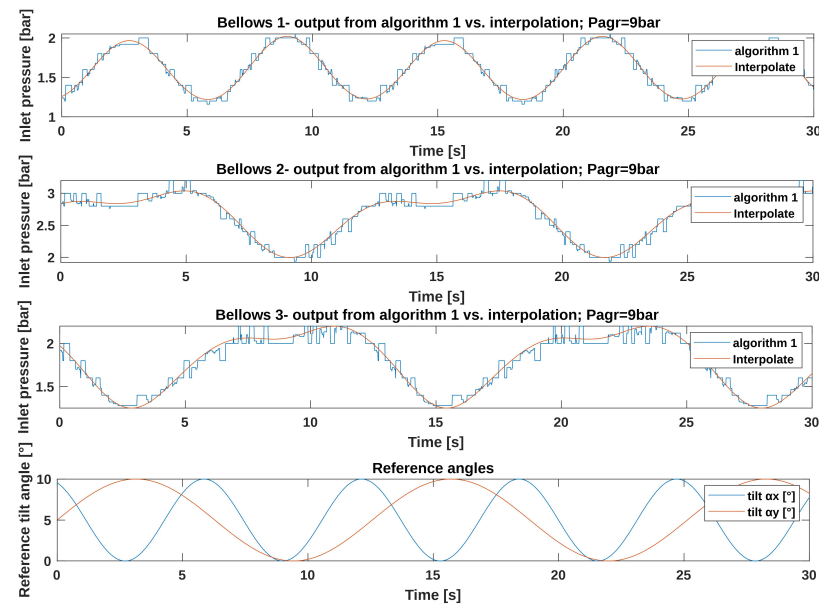


Figure 16. Output from algorithm 1 vs. Interpolation.

4.2. Variable Gain I-Controller Design

The goal of adding an I-part to the controller is to facilitate disturbance rejection by integrating the reference error over time and scaling it by using a gain. In a constant gain I-controller, the gain is tuned to and fixed at a value dependent on the controlled plant. It is simple, easy to implement and does not necessarily require the plant model for correct design and unlike a proportional controller, it allows for complete error compensation in a step response. The problem with using a constant gain I-controller is as follows. The feed-forward controller can immediately supply a rough estimate for input pressures, but

it is never clear before the movement ends how good this estimation is. Therefore, if the estimate is optimal, a constant gain I-controller would cause an overshoot, requiring the controller to be slow. On the other hand, if the estimation is sub-optimal, an aggressive constant gain I-controller is needed to quickly compensate for the error. This contradiction in requirements can be solved by applying a variable gain I-controller, with the gain dependent on the error, see Equation (12)

$$u(t) = K_i(e(t)) \int_0^t e(t) dt \tag{12}$$

where $K_i(e(t))$ is the controller gain, $e(t)$ is the tilt error, t is time and $u(t)$ is the controller output. The idea behind the error-dependent controller gain is to keep the integral action small at the beginning of the movement, before it is clear how good the feed-forward action is, and increase it as the module posture reaches the desired posture. This decreases overshoot while increasing error elimination speed.

The relationship between I-controller gain and tilt error can be described by different types of smooth monotonic functions, like linear, exponential etc. For this controller, as a proof of concept a linear relationship was chosen, see Equation (13).

$$K_i = ae_t(t) + b \tag{13}$$

$$e_t(t) = \sqrt{e_x^2(t) + e_y^2(t)} \tag{14}$$

where $e_t(t)$ is the tilt error, $e_x(t)$ is the tilt error about the x -axis and $e_y(t)$ is the tilt error about the y -axis. Parameters a and b were calculated from experimental data, where $K_i = 350$ was found to work well for small total error values below 1° and $K_i = 75$ was found to not cause significant overshoot at error values above 5° . This relationship is described by Equation (15) and can be seen in Figure 17

$$K_i = -68.75e_t + 418.75 \tag{15}$$

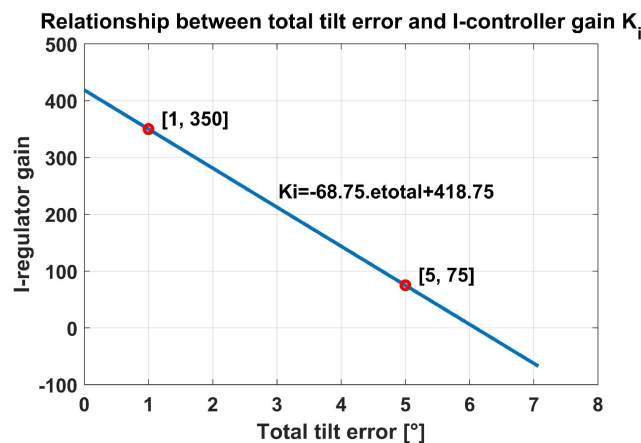


Figure 17. Tilt error in dependence on I-controller gain.

The comparison between the performance of a constant gain I-controller and our variable gain controller in combination with our feed-forward controller is depicted in Figure 18. One can see, that in Figure 18a,b a gain of 350 results in a significant overshoot, but for small changes in tilt and a large residual error after feed-forward controller action, like in Figure 18c, the controller is fast and has acceptable overshoot. On the other hand, a gain of 75 has no overshoot in any case but is slow and has the best performance if the residual error from feed-forward controller action is small, like in Figure 18b. The

performance of both fixed gain controllers in Figure 18c is not satisfactory. Our variable gain controller performs satisfactory in all cases.

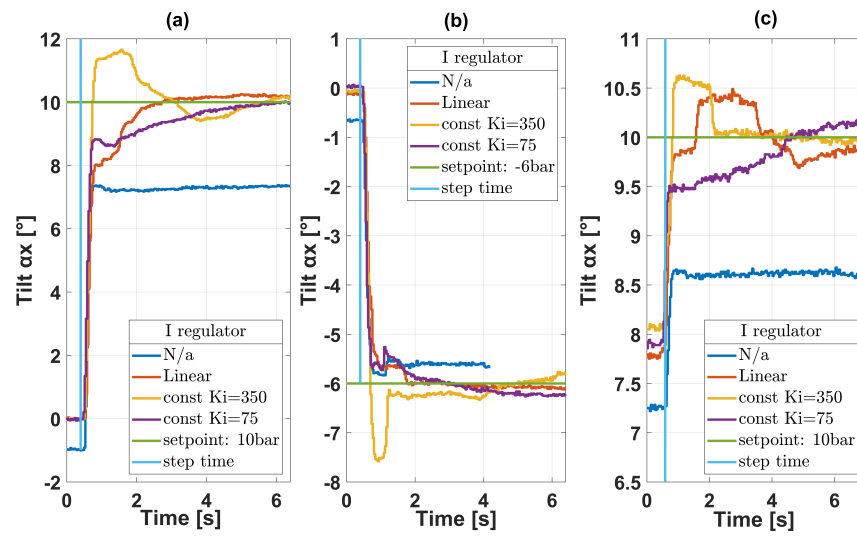


Figure 18. Comparison between constant and variable gain I-controller under different conditions. (a) high feed-forward error; (b) low feed-forward error; (c) reference angle change $\alpha_y = 8^\circ \rightarrow 10^\circ$.

As mentioned above, for our controller, we have chosen a linear relationship to govern the variable gain. A linear relationship is simple, is easy to tune and should result in predictable behaviour of the module. Nevertheless, other types of functions like exponential, polynomial or even logarithmic can also be applied and could result in better controller performance than with a linear equation. The purpose of this article is to show the viability of the presented controller and using a linear relationship for this purpose is sufficient. The complexity of comparing different types of governing equations and the required tuning methods warrants its own article.

5. Experimental Verification of FFvI Controller

This section will focus on the experimental comparison between the FFvI controller and controllers designed according to established algorithms. First of all, the performance of the feed-forward part of the FFvI algorithm will be compared with an ANFIS controller designed using the same data-set as our feed-forward controller. In the second part, the complete FFvI controller will be compared to a constant gain PID controller.

The ANFIS controller was designed using the MATLAB neuro-fuzzy designer. Three controllers for each bellows separately were created. The input data are tilt angles α_x and α_y and the output is the corresponding pressure. The teaching data are picked from the same data, that is used to design the feed-forward controller, but are limited to having an aggregate pressure of 9 ± 1.5 bar. The feed-forward controller is also set to the same level of aggregate pressure. This will decrease the teaching time and ensure more reliable results. The neural network used is a Sugeno-type network [39] with 10 linear generalized bell-shaped membership functions for each input. The minimum achieved teaching error is in Table 2.

Table 2. Minimum teaching error.

Bellows	Teaching Error [bar]
1	0.0205
2	0.0227
3	0.0272

Both controllers were supplied with sets of reference postures and their outputs were compared to input pressures, that produced these postures during measurement. The resulting comparison between the outputs of the feed-forward controller and the ANFIS controller is shown in Figure 19. The minimum error and mean error are in Table 3.

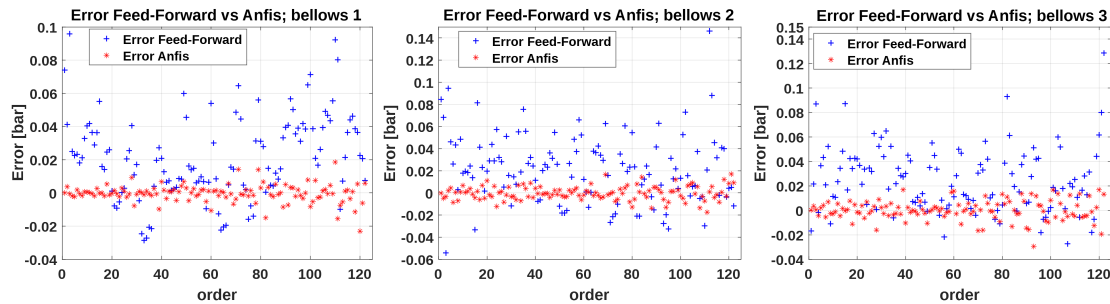


Figure 19. Comparison between feed-forward and ANFIS controller.

Table 3. Maximum error.

Bellows	Controller	Maximum Error [bar]	Mean Error [bar]
1	feed-forward	0.0959	0.0217
	ANFIS	0.0231	−0.0028
2	feed-forward	0.1463	0.0219
	ANFIS	0.0174	−0.0011
2	feed-forward	0.1286	0.025
	ANFIS	0.0294	0.0029

The ANFIS controller has a consistently lower error and the mean error is also lower. Nevertheless, as can be seen from the above results, both controllers perform well, with the maximum error of the feed-forward controller not exceeding 0.15°. The magnitude of this error is still well within what would be considered acceptable for this application. Considering that the feed-forward controller can approximate the whole pressure augmented workspace, while the ANFIS controller is specifically designed to work in the tested aggregate pressure region, these results are encouraging.

When assessing the complete FFvI controller, one must keep in mind that the physical module is meant to be part of a robot. Therefore, we have specified that the overshoot, when performing a movement, should not exceed 2° on α_x and α_y separately. This number, although arbitrary, should be a good controller benchmark for this case and the controller is expected to be further tuned after being installed in the complete robot control system.

As a comparison to our FFvI controller, a PID-based controller was used. The controller consists of three identical constant gain PID controllers controlling all the bellows separately. The PID controllers were tuned using the P-I-D tuning approach described in [40]. It is an experimental method that starts by experimentally tuning the P gain to a satisfactory level while keeping the I gain and D gain at zero. After that, the I gain is calculated according to the step response of the system and the P gain is reduced to retain stability. The D gain can be calculated from the I gain. In this case, the I gain was later increased to speed up the controller, as this method leaves room for improvement in this regard. The D gain was lowered to decrease the effects of noise. The relevant constants can be seen in Table 4. Although the values of the tuned constants are not optimal, the authors believe that they are close enough to the optimal values combining adequate speed while not exceeding our criterion of 2° overshoot on α_x and α_y .

Table 4. PID controller gains.

	Gain Bar/deg
K_P	40
K_I	240
K_D	5

The performance of both controllers can be seen in Figure 20. The reference signal is sequentially alternating between $\alpha_{xref} = 8^\circ$, $\alpha_{yref} = -10^\circ$, $\alpha_{xref} = -8^\circ$ and $\alpha_{yref} = 10^\circ$. These values were chosen because all bellows need to be engaged simultaneously to different degrees, they represent values in the middle part of the module workspace and it is expected that most movements will be within this area. They also demonstrate the asymmetric behavior of the platform.

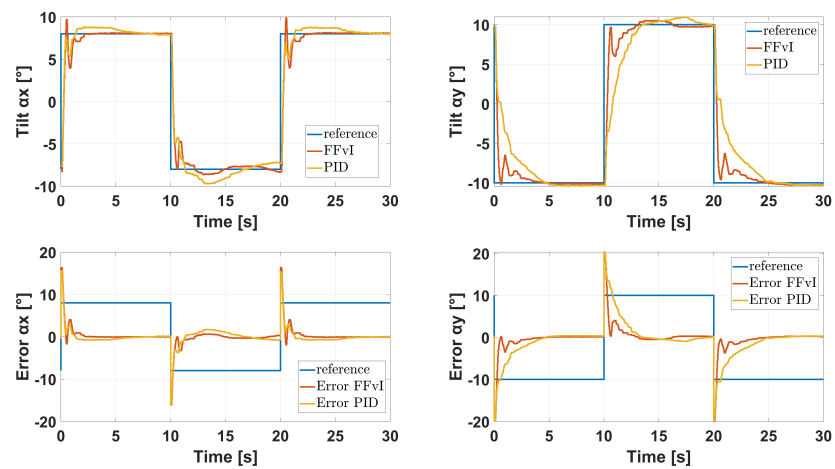


Figure 20. Comparison PID vs. FFvI controller—input step $\alpha_{xref} = -8^\circ$ to 8° ; $\alpha_{yref} = -10^\circ$ to 10° .

The performance of both controller types is shown in Table 5. It needs to be noted that, this comparison deviates from a standard comparison of step responses by not having the platform at zero tilt and testing a combined rotation around α_x and α_y . Nevertheless, this comparison is much closer to comparing the controller performance under more realistic conditions.

It can be seen, that both controllers fulfill the condition of not having more than 2° overshoot. From Table 5 it can be seen, that the FFvI controller is faster in all categories and has more overshoot only when going from $-8^\circ \rightarrow 8^\circ$. The difference in quality between both controllers is illustrated by performance criteria, where in all cases the FFvI controller outperforms the PID controller by roughly more than 40%. The second comparison between both controllers is in following a sine reference signal with parameters written in Table 6, as can be seen in Figure 21. Here the FFvI controller can tightly and smoothly follow the sinusoidal reference signal while overshooting at the maximum and minimum of the reference signal. The overshoot, again, does not exceed 2° for either tilt angles. The PID controller, while not overshooting nearly as much, lags constantly behind the reference signal by about 0.7 s and the plot is in some parts jittery. The overall tracking error is much smaller for the FFvI than for the PID controller. It can be said that both controllers perform acceptably, while the FFvI controller is faster while still passing the overshoot criteria.

Table 5. Performance comparison.

$\alpha_x - 8^\circ \rightarrow 8^\circ$	FFvI	PID	$\alpha_y 10^\circ \rightarrow -10^\circ$	FFvI	PID
rise time [s]	0.42	0.4	rise time [s]	2.74	4.13
settling time 5% [s]	2.03	5.42	settling time 5% [s]	3.43	4.5
first maximum [s]	0.54	2.15	first maximum [s]	0.65	7.45
overshoot [%]	21.1	10.3	overshoot [%]	3	3
$\alpha_x 8^\circ \rightarrow -8^\circ$	FFvI	PID	$\alpha_y - 10^\circ \rightarrow 10^\circ$	FFvI	PID
rise time [s]	0.5	1.23	rise time [s]	0.53	3
settling time 5% [s]	4.46	5<	settling time 5% [s]	2.73	8.04
first maximum [s]	0.57	3.4	first maximum [s]	0.64	7.5
overshoot [%]	8	21.3	overshoot [%]	5	9.6
performance criteria	FFvI	PID			
IAE	40.9	79.3			
ISE	461.9	758.2			
ITAE	481.2	954.1			

Table 6. Sinus reference signal parameters.

Sinus Signal	α_{xref}	α_{yref}
amplitude [°]	10	10
period [s]	2π	2π
phase [rad]	0	$\pi/2$
bias [°]	0	0

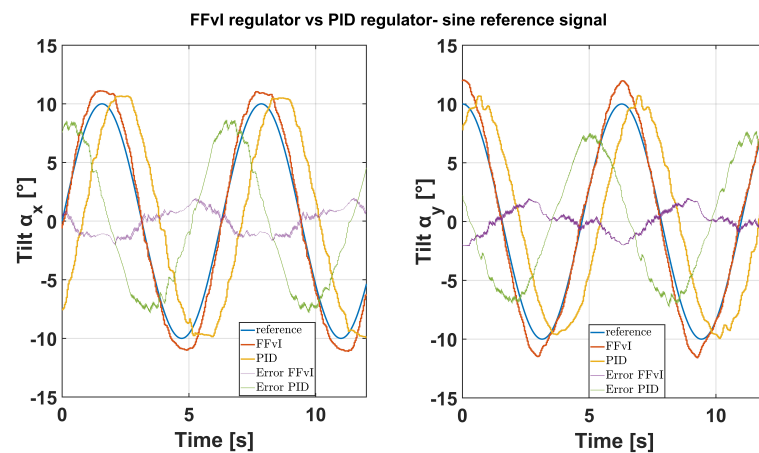


Figure 21. Comparison PID controller vs. FFvI controller—input sinus wave.

One ability that the FFvI controller has is to change the stiffness of the system while maintaining reference posture. Stiffness is set indirectly by inputting a number between 1–15 bar. This number represents the sum of the input pressures in all bellows and correlates with the overall stiffness of the system. The reason we did not quantify the stiffness is because stiffness is not only dependent on the input pressure, but also on the posture of the module making stiffness a three-dimensional matrix of values. This makes it impractical as an intuitive value that should be specified by the user. An algorithm to convert stiffness to aggregate pressure can be designed, but it would not change any part of the controller. The ability to change the stiffness during operation is shown in Figure 22. The module is first positioned to $\alpha_{xref} = 10^\circ$, $\alpha_{yref} = 5^\circ$ at a requested aggregate pressure of 3 bar. Then, the aggregate pressure is changed step-wise to 6 bar, 9 bar, 12 bar and 15 bar, respectively. A change in aggregate pressure corresponds to a change in the stiffness of the system. As seen from Figure 22, the pressure and therefore stiffness can be changed online. This change

produces a momentous destabilization of the system resulting in slight position loss. The maximum error for our test was at the transition between aggregate pressure 12 bar and 15 bar with maximum error for $\alpha_{xref} = 1.3^\circ$, $\alpha_{yref} = 1.65^\circ$. This can be again, attributed to nonsynchronous pressure change between the bellows and possible measurement errors in the original feed-forward controller input data. Therefore, instead of a sharp aggregate pressure step a smooth aggregate pressure transition should decrease this issue.

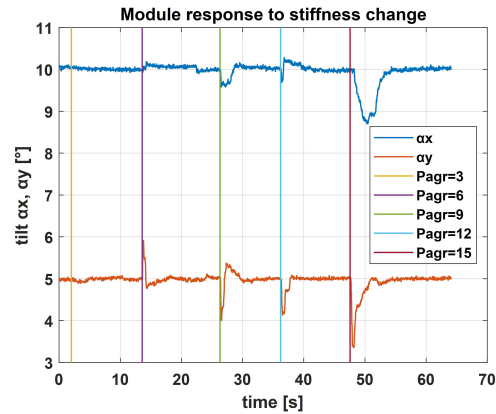


Figure 22. Module response to stiffness change.

6. Dynamic Test of Ffvi Tilt Platform Controller

To be able to apply the proposed controller as part of the control system of the whole manipulator it is necessary to test the controller under dynamic loading conditions.

For this purpose, a two-axis loading mechanism was developed, see Figure 23. It consists of two linear motion axes stacked perpendicular on top of each other and a weight attached to the top axis. This mechanism is mounted on top of a tilt module with the axis of the platform aligned with the linear motion axes of the mechanism. It can be seen that the potential loading momentum will be different for each axis because the bottom axis is loaded not only by the loading weight but also by the top axis itself. The possible motion of one linear axis is 0 mm to 330 mm and is centered on the central axis of the tilt module. The weight of the axes and loading weight is in Table 7. This mechanism is used to generate dynamic loading forces to study the capability of the FFvI controller to reject dynamic disturbances.

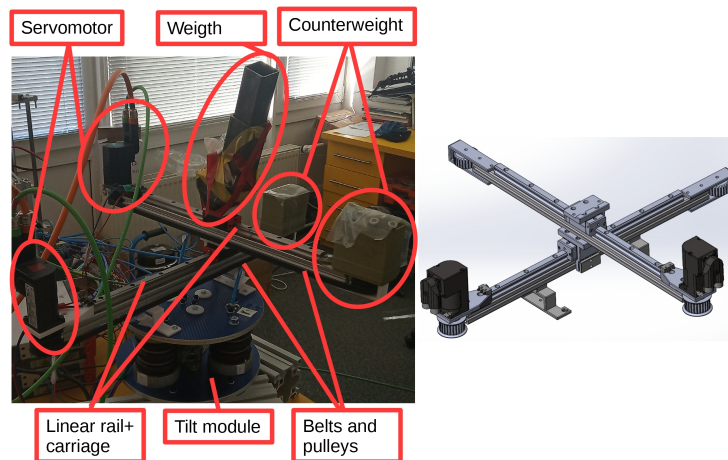


Figure 23. Dynamic two axis loading mechanism.

Table 7. Loading weights.

	Weight [g]
linear axis	2467
loading weight	1802

The dynamic loading experiment is done for reference tilts $\alpha_x = 0^\circ$ and $\alpha_y = 0^\circ$. Error rejection is facilitated by the I controller part of the algorithm, hence the test will be performed with the I controller active and, for comparison, with the I controller inactive. In addition, the experiment will be done for different values of aggregate pressure and for different speeds of movement of the loading weight. The movement of the load was converted to loading momentum about axes x and y (see Figure 24). Figures 24 and 25 show only the extremes of the test, different combinations of load speed and aggregate pressure were also tested, see Table 8.

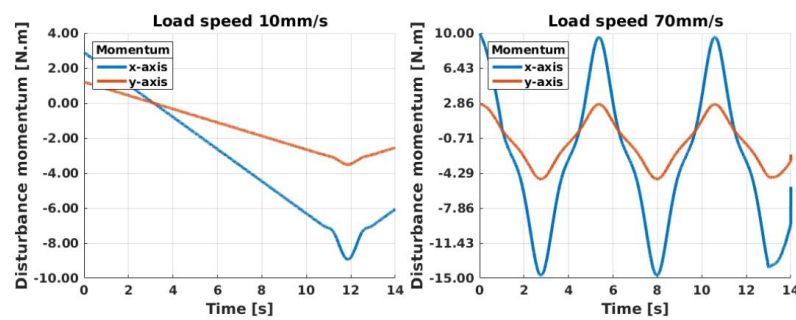


Figure 24. Disturbance momentum at different loading speeds.

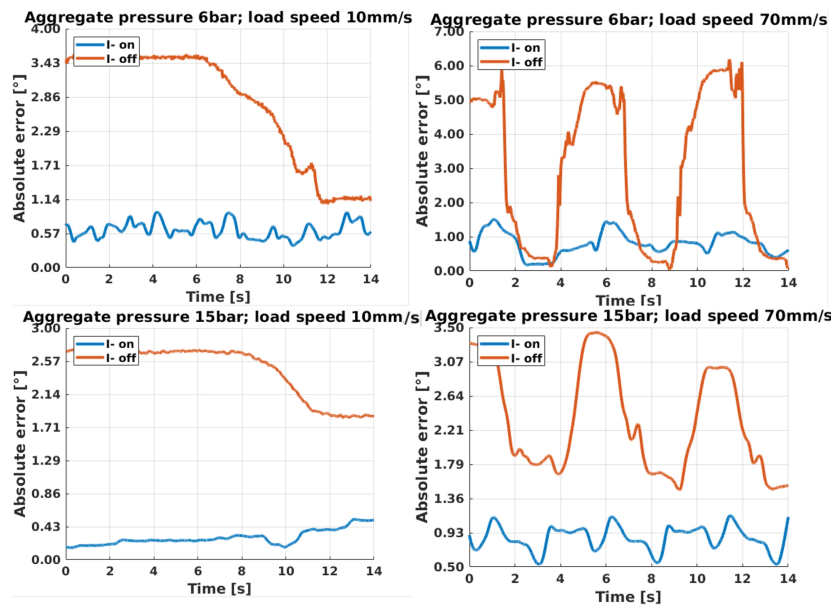


Figure 25. Comparison between active and inactive I regulator at tilt holding at extreme aggregate pressures and dynamic effects.

The disturbance momentum was indirectly established from the measured movement of the load and the geometry of the mechanism. The shown time window is the same for all movement speeds. The maximum total error for all measurements is in Table 8.

Table 8. Maximum total error under dynamic load.

Velocity; Pressure	I on [°]	I off [°]
10 mm/s; 6 bar	0.93	3.57
30 mm/s; 6 bar	0.66	4.29
50 mm/s; 6 bar	1.52	3.48
70 mm/s; 6 bar	1.51	6.18
10 mm/s; 9 bar	0.31	3.84
30 mm/s; 9 bar	0.62	3.75
50 mm/s; 9 bar	1.02	3.66
70 mm/s; 9 bar	1.05	6.82
10 mm/s; 12 bar	0.28	2.78
30 mm/s; 12 bar	0.60	2.58
50 mm/s; 12 bar	0.88	3.17
70 mm/s; 12 bar	1.15	5.42
10 mm/s; 15 bar	0.52	2.74
30 mm/s; 15 bar	0.63	2.68
50 mm/s; 15 bar	0.87	3.24
70 mm/s; 15 bar	1.14	3.44
mean	0.86	3.85

From the above figures, one can deduce important findings regarding the behaviour of the controller under dynamically changing load. The maximum total error with the I part active was 1.52° and the mean error was 0.86° and the maximum total error with the I part inactive was 6.85° and the mean error was 3.85° . Apart from that, a well-tuned variable gain I-controller has a significant stabilisation effect at higher dynamic loads. It can also be seen, especially at higher speeds of the load, that a higher aggregate pressure has a positive effect on the rejection of dynamic loads.

It can be concluded that the FFvI controller in its current state is able to control the prototype manipulator, especially at lower speeds and higher aggregate pressure settings.

7. Discussion

In this paper, a new type of controller for the control of the posture of a pneumatic bellows actuated module of the cascade robot PneuTrunk was presented. The controller consists of a feed-forward controller designed using experimental data and a error dependent variable gain I-controller. The feed-forward controller is created by fitting the data at a certain pressure level using a polynomial function and subsequently, again fitting the resulting set of polynomial function constants by another set of polynomials. This allows for a simple and fast controller, that not only allows to control the posture of the module, but also its stiffness. The variable gain I-controller supplements the feed-forward controller by adding a feedback loop, hence facilitating disturbance rejection and correcting for feed-forward controller imperfections. The variable gain allows for fast error correction while limiting overshoot and windup at the same time. This hybridisation approach allows for a simple controller design for a complex MIMO systems that can be easily adjusted and updated.

This controller was compared to other established controllers. On the feed-forward level, the controller was compared with an ANFIS controller, delivering comparable results. Comparing the complete controller to a tuned PID controller showed that our FFvI controller is faster, and can reliably follow a harmonic reference signal while maintaining required performance parameters. This controller was also tested under dynamic load with satisfactory results. The maximum FFvI controller error during the positioning of the module with consideration of dynamic disturbance was only 1.52° . The aforementioned tests show a robust behaviour of the FFvI controller in the face of both internal feed-forward model imperfections, as shown by quick error rejection in the step response tests and external dynamic disturbance forces, as shown by the dynamic tests.

To further improve the performance of the controller, it is necessary to create a comprehensive mathematical model of the module, mainly to combat the detrimental effects of the hysteretic behavior of the bellows. It is also appropriate to compare different types of functions driving the variable gain of the I-controller. In the future, this controller will be applied as a part of a larger control system controlling the pneumatic cascade robot PneuTrunk.

Author Contributions: M.V.—Investigation and Formal analysis; I.V.—Project administration; M.K.—Supervision; L.M.—Methodology; Z.B.—Validation; P.J.S. and T.M.—Software. All authors have read and agreed to the published version of the manuscript.

Funding: This research was funded by Slovak Grant Agency VEGA 1/0436/22 Research on modelling methods and control algorithms of kinematically redundant mechanisms and VEGA 1/0201/21 Mobile mechatronic assistant. This research has been also elaborated under the support of the project Research Centre of Advanced Mechatronic Systems, reg. No. CZ.02.1.01/0.0/0.0/16019/0000867 in the frame of the Operational Program Research, Development and Education.

Institutional Review Board Statement: Not applicable.

Informed Consent Statement: Not applicable.

Data Availability Statement: The data presented in this study are available on request from the corresponding author. The data are not publicly available due to funding project restrictions.

Acknowledgments: We appreciate the support of all members of ARM-lab and the Prototyping laboratory at the Faculty of mechanical engineering of the Technical university of Košice.

Conflicts of Interest: The authors declare no conflict of interest.

Abbreviations

The following abbreviations are used in this manuscript:

ANFIS	Adaptive neuro fuzzy inference system
ARM-Lab	Applied Robotics and Mechatronics Laboratory
FFvI	Feed-forward variable gain integral controller
MIMO	Multi input multi output system
PID	Proportional–integral–derivative controller
SMA	Shape memory alloy
SMC	sliding mode controller
IAE	Integral of the absolute error
ISE	Integral of the squared error
ITAE	Integral of time multiplied by absolute error

References

1. Gregov, G.; Ploh, T.; Kamenar, E. Design, Development and Experimental Assessment of a Cost-Effective Bellow Pneumatic Actuator. *Actuators* **2022**, *11*, 170. [[CrossRef](#)]
2. Kelemen, M.; Virgala, I.; Liptak, T.; Mikova, L.; Filakovsky, F.; Bulej, V. A Novel Approach for a Inverse Kinematics Solution of a Redundant Manipulator. *Appl. Sci.* **2018**, *8*, 2229. [[CrossRef](#)]
3. Virgala, I.; Kelemen, M.; Varga, M.; Kurylo, P. Analyzing, Modeling and Simulation of Humanoid Robot Hand Motion. *Procedia Eng.* **2014**, *96*, 489–499. [[CrossRef](#)]
4. Hroncová, D.; Sinčák, P.J.; Merva, T.; Mykhalyshyn, R. Robot trajectory planning. *MM Sci. J.* **2022**. [[CrossRef](#)]
5. Chirikjian, G.; Burdick, J. Hyper-redundant robot mechanisms and their applications. In Proceedings of the Proceedings IROS'91:IEEE/RSJ International Workshop on Intelligent Robots and Systems '91, Osaka, Japan, 3–5 November 1991; Volume 1, pp. 185–190. [[CrossRef](#)]
6. Chirikjian, G.; Burdick, J. A hyper-redundant manipulator. *IEEE Robot. Autom. Mag.* **1994**, *1*, 22–29. [[CrossRef](#)]
7. Zhao, Y.; Song, X.; Zhang, X.; Lu, X. A Hyper-redundant Elephant's Trunk Robot with an Open Structure: Design, Kinematics, Control and Prototype. *Chin. J. Mech. Eng.* **2020**, *33*, 96. [[CrossRef](#)]
8. Grace, D.; Lee-Ortiz, J.; Garcia, M.; Contreras-Esquen, A.; Tekes, A.; Amiri Moghadam, A.A. Development of a Novel Six DOF Soft Parallel Robot. In Proceedings of the SoutheastCon 2022, Mobile, AL, USA, 26 March–3 April 2022; pp. 81–86. [[CrossRef](#)]

9. Pi, Y.; Wang, X. Trajectory tracking control of a 6-DOF hydraulic parallel robot manipulator with uncertain load disturbances. *Control. Eng. Pract.* **2011**, *19*, 185–193. [[CrossRef](#)]
10. Cheng, C.; Cheng, J.; Huang, W. Design and Development of a Novel SMA Actuated Multi-DOF Soft Robot. *IEEE Access* **2019**, *7*, 75073–75080. [[CrossRef](#)]
11. Wingert, A.; Lichter, M.D.; Dubowsky, S.; Hafez, M. Hyper-redundant robot manipulators actuated by optimized binary-dielectric polymers. In Proceedings of the SPIE Smart Structures and Materials + Nondestructive Evaluation and Health, Monitoring, San Diego, CA, USA, 18–19 March 2002.
12. Nall, C.L.; Bhounsule, P.A. A Miniature 3D Printed On-Off Linear Pneumatic Actuator and Its Demonstration into a Cartoon Character of a Hopping Lamp. *Actuators* **2019**, *8*, 72. [[CrossRef](#)]
13. Tao, G.; Shang, C.; Meng, D. Adaptive Robust Posture Control of a 3-RPS Pneumatic Parallel Platform with Unknown Deadzone. *Math. Probl. Eng.* **2016**, *2016*, 2034923. [[CrossRef](#)]
14. Trebuna, F.; Kelemen, M.; Pastor, M.; Virgala, I. Trajectory Tracking Controller of Air Bellow. *J. Autom. Control* **2016**, *4*, 51–55. [[CrossRef](#)]
15. Gryparis, D.; Andrikopoulos, G.; Manesis, S. Parallel robotic manipulation via Pneumatic Artificial Muscles. In Proceedings of the 2014 11th International Conference on Informatics in Control, Automation and Robotics (ICINCO), Vienna, Austria, 1–3 September 2014; Volume 2, pp. 29–36. [[CrossRef](#)]
16. Wang, Y.; Xu, Q. Design and testing of a soft parallel robot based on pneumatic artificial muscles for wrist rehabilitation. *Sci. Rep.* **2021**, *11*, 1273. [[CrossRef](#)] [[PubMed](#)]
17. Cianchetti, M.; Ranzani, T.; Gerboni, G.; De Falco, I.; Laschi, C.; Menciassi, A. STIFF-FLOP surgical manipulator: Mechanical design and experimental characterization of the single module. In Proceedings of the 2013 IEEE/RSJ International Conference on Intelligent Robots and Systems, Tokyo, Japan, 3–7 November 2013; pp. 3576–3581. [[CrossRef](#)]
18. Garbin, N.; Wang, L.; Chandler, J.H.; Obstein, K.L.; Simaan, N.; Valdastrì, P. A disposable continuum endoscope using piston-driven parallel bellow actuator. In Proceedings of the 2018 International Symposium on Medical Robotics (ISMR), Atlanta, GA, USA, 1–3 March 2018; pp. 1–6. [[CrossRef](#)]
19. Gong, Z.; Chen, B.; Liu, J.; Fang, X.; Liu, Z.; Wang, T.; Wen, L. An Opposite-Bending-and-Extension Soft Robotic Manipulator for Delicate Grasping in Shallow Water. *Front. Robot. AI* **2019**, *6*, 26. [[CrossRef](#)] [[PubMed](#)]
20. Liu, Z.; Karydis, K. Position Control and Variable-Height Trajectory Tracking of a Soft Pneumatic Legged Robot. In Proceedings of the 021 IEEE/RSJ International Conference on Intelligent Robots and Systems (IROS), Prague, Czech Republic, 27 September–1 October 2021.
21. Granosik, G.; Kaczmarek, M. Bellows Driven, Muscle Steered Caterpillar Robot. In *Climbing and Walking Robots: Proceedings of the 8th International Conference on Climbing and Walking Robots and the Support Technologies for Mobile Machines (CLAWAR 2005)*; Tokhi, M.O., Virk, G.S., Hossain, M.A., Eds.; Springer: Berlin/Heidelberg, Germany, 2006; pp. 743–750.
22. Fujita, T.; Sakai, K.; Takagi, Y.; Kawashima, K.; Kagawa, T. Ultra Precise Positioning of a Stage Driven by Pneumatic Bellows. *Int. J. Autom. Technol.* **2011**, *5*, 508–515. [[CrossRef](#)]
23. Harsono, E.; Yang, J.; Bhattacharya, S.; Yu, H. Design and analysis of a novel hybrid-driven continuum robot with variable stiffness. *Mech. Mach. Theory* **2022**, *177*, 105067. [[CrossRef](#)]
24. Fortuna, L.; Frasca, M.; Buscarino, A. *Optimal and Robust Control: Advanced Topics with MATLAB®*, 2nd ed.; CRC Press: Boca Raton, FL, USA, 2021. [[CrossRef](#)]
25. Huang, X.; Zhu, X.; Gu, G. Kinematic Modeling and Characterization of Soft Parallel Robots. *IEEE Trans. Robot.* **2022**, *38*, 1–15. [[CrossRef](#)]
26. Zhang, J.; Wei, H.; Shan, Y.; Li, P.; Zhao, Y.; Qi, L.; Yu, H. Modeling and Experimental Study of a Novel Multi-DOF Parallel Soft Robot. *IEEE Access* **2020**, *8*, 62932–62942. [[CrossRef](#)]
27. Calabria, M.; Schreiber, F.; Sklyarenko, Y.; Inkermann, D.; Raatz, A.; Vietor, T.; Schumacher, W. Redundancy resolution and control of manipulators driven by antagonistic pneumatic muscles. In Proceedings of the 2012 17th International Conference on Methods & Models in Automation & Robotics (MMAR), Miedzyzdroje, Poland, 27–30 August 2012; pp. 119–124. [[CrossRef](#)]
28. Katzschmann, R.K.; Santina, C.D.; Toshimitsu, Y.; Bicchi, A.; Rus, D. Dynamic Motion Control of Multi-Segment Soft Robots Using Piecewise Constant Curvature Matched with an Augmented Rigid Body Model. In Proceedings of the 2019 2nd IEEE International Conference on Soft Robotics (RoboSoft), Seoul, Republic of Korea, 14–18 April 2019; pp. 454–461. [[CrossRef](#)]
29. Falkenhahn, V.; Hildebrandt, A.; Neumann, R.; Sawodny, O. Model-based feedforward position control of constant curvature continuum robots using feedback linearization. In Proceedings of the 2015 IEEE International Conference on Robotics and Automation (ICRA), Seattle, WA, USA, 25–30 May 2015; pp. 762–767. [[CrossRef](#)]
30. Khoa, L.D.; Truong, D.Q.; Ahn, K.K. Synchronization controller for a 3-R planar parallel pneumatic artificial muscle (PAM) robot using modified ANFIS algorithm. *Mechatronics* **2013**, *23*, 462–479. [[CrossRef](#)]
31. Khan, A.H.; Li, S. Sliding Mode Control With PID Sliding Surface for Active Vibration Damping of Pneumatically Actuated Soft Robots. *IEEE Access* **2020**, *8*, 88793–88800. [[CrossRef](#)]
32. Chiang, M.H.; Lin, H.T. Development of a 3D Parallel Mechanism Robot Arm with Three Vertical-Axial Pneumatic Actuators Combined with a Stereo Vision System. *Sensors* **2011**, *11*, 11476–11494. [[CrossRef](#)]
33. Mo, H.; Li, X.; Ouyang, B.; Fang, G.; Jia, Y. Task Autonomy of a Flexible Endoscopic System for Laser-Assisted Surgery. *Cyborg Bionic Syst.* **2022**, *2022*, 9759504. [[CrossRef](#)]

34. Ateş, A.; Alagöz, B.B.; Yeroğlu, C.; Alisoy, H. Sigmoid based PID controller implementation for rotor control. In Proceedings of the 2015 European Control Conference (ECC), Linz, Austria, 15–17 July 2015; pp. 458–463. [[CrossRef](#)]
35. Suid, M.H.; Ahmad, M.A. Optimal tuning of sigmoid PID controller using Nonlinear Sine Cosine Algorithm for the Automatic Voltage Regulator system. *ISA Trans.* **2022**, *128*, 265–286. [[CrossRef](#)] [[PubMed](#)]
36. Yeh, Y.L.; Yang, P.K. Design and Comparison of Reinforcement-Learning-Based Time-Varying PID Controllers with Gain-Scheduled Actions. *Machines* **2021**, *9*, 319. [[CrossRef](#)]
37. Lakhal, O.; Melingui, A.; Chibani, A.; Escande, C.; Merzouki, R. Inverse Kinematic modeling of a class of continuum bionic handling arm. In Proceedings of the 2014 IEEE/ASME International Conference on Advanced Intelligent Mechatronics, Besançon, France, 8–11 July 2014; pp. 1337–1342. [[CrossRef](#)]
38. Mishra, M.K.; Samantaray, A.K.; Chakraborty, G. Fractional-order Bouc-wen hysteresis model for pneumatically actuated continuum manipulator. *Mech. Mach. Theory* **2022**, *173*, 104841. [[CrossRef](#)]
39. Takagi, T.; Sugeno, M. Fuzzy identification of systems and its applications to modeling and control. *IEEE Trans. Syst. Man Cybern.* **1985**, *SMC-15*, 116–132. [[CrossRef](#)]
40. Haugen, F. *PID Control*; Tapir Academic Press: Trondheim, Norway, 2004; ISBN 978-8251919456.

Disclaimer/Publisher’s Note: The statements, opinions and data contained in all publications are solely those of the individual author(s) and contributor(s) and not of MDPI and/or the editor(s). MDPI and/or the editor(s) disclaim responsibility for any injury to people or property resulting from any ideas, methods, instructions or products referred to in the content.